Quantum molecular dynamics simulations of transport properties in liquid and dense-plasma plutonium

J. D. Kress, James S. Cohen, D. P. Kilcrease, D. A. Horner, and L. A. Collins

Phys. Rev. E **83**, 026404 — Published 16 February 2011

DOI: 10.1103/PhysRevE.83.026404

Quantum molecular dynamics simulations of transport properties in liquid and dense-plasma plutonium

J. D. Kress,[1] James S. Cohen,[1] D. P. Kilcrease,[1] D. A. Horner,[1] and L. A. Collins[1]

[1] *Theoretical Division, Los Alamos National Laboratory, Los Alamos, New Mexico 87545*

Abstract

We have calculated the viscosity and self-diffusion coefficients of plutonium in the liquid phase using quantum molecular dynamics (QMD) and in the dense-plasma phase using orbital-free molecular dynamics (OFMD), as well as in the intermediate warm dense matter regime with both methods. Our liquid metal results for viscosity are about 40% lower than measured experimentally, whereas a previous calculation using an empirical interatomic potential (modified embedded atom method) obtained results 3 to 4 times larger than the experiment. The QMD and OFMD results agree well at the intermediate temperatures. The calculations in the dense-plasma regime for temperatures from 50 to 5000 eV and densities about 1–5 times ambient are compared with the one-component plasma (OCP) model, using effective charges given by the average-atom code INFERNO. The OCP/INFERNO model results agree with the OFMD to within about a factor of two, except for the viscosity at temperatures less than about 100 eV where the disagreement is greater. A Stokes-Einstein relationship of the viscosities and diffusion coefficients is found to hold fairly well separately in both the liquid and dense-plasma regimes.

[LANL publication number: LA-UR-10-07728]

PACS numbers: 52.25.Fi,52.65.Yy,52.27.Gr

I. INTRODUCTION

Plutonium (Pu) ranks as the heaviest naturally occurring element, given its presence in trace amounts within uranium ores. It has several atypical properties when compared to standard metals [1, 2]. Plutonium has a very low melt temperature (913 K) and contracts while melting, a property shared with water and some semimetals, has poor electrical and thermal conduction characteristics, but has good elastic compressibility. Six allotropes exist in the solid form that exhibit a variety of different structures and properties. For example, the α phase expands much faster than iron on heating while the δ phase contracts. These peculiarities can be attributed to the location of Pu at a transition point between itinerant and localized $5f$ electrons. The unusual behavior of the substance does not cease at melt. As a liquid, plutonium has a high surface tension and one of the largest viscosities of any metal, although in actual flow its mass somewhat ameliorates this distinction. While most noted in its role in nuclear explosions, plutonium has many applications, e.g. supplying the heating element in radioisotope thermoelectric generators used in remote sensing stations and deep-space craft such as Cassini and forming a principal component in closed fuel cycles for fast nuclear reactors as part of advanced energy initiatives [1].

In contrast to the the extensive experimental, theoretical, and computational efforts to elucidate the material properties of the solid allotropes [3], the liquid phase has remained relatively unexplored except around the melt temperature, due to its highly reactive, corrosive, and radioactive nature. Measurements [4] of the shear viscosity exist up to 1500 K as well as of various optical properties [5]. In addition, the viscosities of some liquid Pu alloys, including U-Pu, have been determined [4, 6, 7]. A few theoretical studies exist; for example, simulations with the modified embedded-atom method (MEAM), which utilizes an angle-dependent empirical interatomic potential, appear for liquid plutonium [8] as well as nickel [9], but only near melt.

Given the paucity of information above melt, we have employed molecular dynamics simulation techniques to determine the transport properties, both diffusion and viscosity, of Pu from the liquid, through the warm, dense matter (WDM) regime, to the plasma over a broad range of temperatures [up to 5 keV] and compressions [1–5 times solid]. The WDM regime, although somewhat ill-defined, spans a range of densities between 1/100 and 100 times solid and temperatures from about 1 eV to several hundred eV and marks a region

that resembles a soup of various particle types including atoms, ions, free electrons, and even molecules in a highly transient state for which a quantum mechanical treatment obtains. As the temperature rises and ionization increases, the particle interactions become more classical, signaling the beginning of a conventional plasma environment. To examine this broad range of conditions, we applied quantum molecular dynamics (QMD) and orbital-free molecular dynamics (OFMD) simulations, both of which treat the electrons quantum mechanically and the nuclei classically. The QMD method employs a finite-temperature Kohn-Sham density-functional theory. QMD simulations of shear viscosity first appeared over a decade ago for liquid Al [10] and a liquid Fe/S alloy [11] at conditions found within the Earth's core. The large computational requirements of QMD generally restrict its applications to relatively low temperatures. Through the use of gradient-corrected, non-local kinetic energy functionals, orbital-free density-functional calculations [12] have accurately simulated solids, like Al and Si, at room temperature. For this study, we restrict the OFMD to a semiclassical formulation at the Thomas-Fermi-Dirac level, which permits its extension to much higher temperatures and densities. Previous investigations on such diverse systems as hydrogen [13, 14], iron [15], gold [16], and lithium hydride [17] have demonstrated that for static (equation-of-state), transport, and optical properties the semi-classical OFMD generally agrees well with QMD in intermediate temperature and density regimes and can effectively reach very high temperatures (~ 5 keV). We also investigate the validity of the Stokes-Einstein relationship between diffusion and viscosity as well as compare our results with the one-component-plasma (OCP) model, using effective charges obtained with the code INFERNO [18].

The remainder of the paper is organized as follows: Section II describes the QMD and OFMD methods, the prescriptions for determining the transport coefficients, and the modified OCP model; Section III presents the results and discussion of the various findings; and Section IV concludes with a brief summary.

II. FORMALISM

A. Quantum molecular dynamics

The QMD simulations employed the Vienna *ab-initio* Simulation Package (VASP) [19–21], in which the electrons are treated fully quantum mechanically using a plane-wave finite-temperature density-functional-theory (FTDFT) description. The electron-ion interaction is represented by a projector augmented wave (PAW) pseudopotential. The ions are evolved classically according to the forces due to the electron density and the ion-ion repulsion. The molecular dynamics is performed in the isokinetic ensemble. The system is assumed to be in local thermodynamic equilibrium with the electron and ion temperatures equal ($T_e = T_i = T$). In our simulations, the electron temperature is fixed, and the ion temperature is kept at this value through simple velocity rescaling (Woodcock thermostat) [22].

At each time step t for a periodically-replicated cubic cell of length L and volume L^3 containing N_e active electrons and N_i ions in fixed spatial positions $\mathbf{R}(t)$, we first perform a FTDFT calculation within the Kohn-Sham (KS) construction [23] to determine a set of electronic state functions $[\Psi_{i,\mathbf{k}}(\mathbf{r},t)|i = 1, N_b]$ and eigenenergies $\epsilon_{i,\mathbf{k}}$ at each k-point $\mathbf{k}$,

$$H_{\rm KS}\Psi_{i,\mathbf{k}}(\mathbf{r},t) = \epsilon_{i,\mathbf{k}}\Psi_{i,\mathbf{k}}(\mathbf{r},t) \tag{1}$$

where in atomic units

$$H_{\rm KS} = -\frac{1}{2}\nabla^2 + V_{\rm ext}(\mathbf{r}) + \int \frac{n_e(\mathbf{r}')}{|\mathbf{r}-\mathbf{r}'|}d\mathbf{r}' + V_{\rm xc}(\mathbf{r}) \tag{2}$$

with electron number density

$$n_e(\mathbf{r}) = \sum_i f_i|\Psi_{i,\mathbf{k}}(\mathbf{r},t)|^2 \tag{3}$$

for the occupation number f_i determined by a Fermi-Dirac distribution at a prescribed electron temperature T_e. The terms in Eq. (2) represent the kinetic energy, the external or electron-ion interaction, the Hartree contribution to the electronic energy, and the exchange-correlation potential, respectively.

The ions are then advanced with a velocity Verlet algorithm, based on the forces due to the other ions and electronic density, to obtain a new set of positions and velocities. Repetition of these two steps propagates the system in time yielding a trajectory consisting

of the positions and velocities $[\mathbf{R}(t), \mathbf{V}(t)]$ of the ions and a collection of state functions $[\Psi_{i,\mathbf{k}}(\mathbf{r}, t)]$ for the electrons.

All our simulations employed only Γ point ($\mathbf{k}$ =0) sampling of the Brillouin zone and 54 atoms (N_i) in the cubic cell (with atomic number density $n_i = N_i/L^3$). The mass density is calculated using atomic weight A=244 g/mol for Pu. We solve the KS equations within the generalized gradient approximation (GGA) [24] and describe the plutonium-electron interaction with a PAW potential for sixteen active electrons with a maximum energy cutoff of 254 eV. A sufficient number N_b of bands was included such that the occupation of the highest band was less than 10^{-2}. Trajectories were evolved with time steps of 2.5 or 5.0 fs.

Plutonium metal has earned a reputation for being the most complex and anomalous element in the periodic table. The δ-phase (fcc structure), which transforms from γ-phase at $T = 593$ K, has an astounding 25% larger atomic volume than the ground state α-phase (monoclinic structure, $\rho_0 = 19.82$ g/cm^3, $V = 19.46$ $\mathring{A}^3$/atom [25]). The electronic structure for solid Pu at $T = 0$ K encompasses both localized and itinerant $5f$ electrons. The state of affairs for electronic structure calculations for solid Pu has been recently summarized by Rudin [3]. Non-spin-polarized DFT in the GGA yields structural data for α-Pu in good agreement with experiment. To successfully describe hypothetical (not experimentally observed) δ-Pu at $T = 0$ K requires enhancements to non-spin-polarized DFT/GGA, such as the mixed level models [26] and dynamic mean field theory [27]. Similar success can be obtained when spin-polarized DFT/GGA is used to introduce magnetic moments. The spin polarization emulates the effects of electron-electron correlation in localized $5f$ states. An anti-ferromagnetic spin density describes [28] the equilibrium volumes and bulk modulus of δ-Pu well. For example, $V = 23.2$ $\mathring{A}^3$/atom vs. $V = 24.93$ $\mathring{A}^3$/atom, the value obtained [25] from the analysis of the experimental thermodynamical data for the six crystalline phases of Pu. This result predicted by simulation has sparked a vigorous debate as no magnetic moment has been observed [29] for δ-Pu. However, when the δ-Pu is "melted" in the QMD simulations, we find that the resulting short-range disorder in the fluid and the finite temperature electrons (FTDFT) yield a non-magnetic ground state for temperatures above $T = 0.15$ eV. Thus for consistency in the comparisons, we use non-spin-polarized DFT for all of the QMD simulations in the present work.

B. Orbital free molecular dynamics

In OFMD simulations [15, 30–32], the kinetic energy of the electrons is treated in a semiclassical approximation, up to first order in the partition function of the electrons. The orbital-free procedure treats all electrons on an equal footing, albeit approximately, with no distinction between bound and ionized electrons. The orbital-free electronic free energy at ion positions $\mathbf{R}$ is given by

$$\begin{aligned} F_e\big[\mathbf{R}, n_e\big] = \frac{1}{\beta}\int \mathrm{d}\mathbf{r}\left(n_e(\mathbf{r})\Phi[n_e(\mathbf{r})] - \frac{2\sqrt{2}}{3\pi^2\beta^{\frac{3}{2}}} I_{\frac{3}{2}}\big(\Phi[n_e(\mathbf{r})]\big)\right) \\ + \int \mathrm{d}\mathbf{r}\, V_{ext}(\mathbf{r}) n_e(\mathbf{r}) + \frac{1}{2}\iint \mathrm{d}\mathbf{r}\mathrm{d}\mathbf{r}'\, \frac{n_e(\mathbf{r}) n_e(\mathbf{r}')}{|\mathbf{r}-\mathbf{r}'|} + F_{xc}[n_e] \end{aligned} \tag{4}$$

where $\beta = 1/k_B T$ (k_B is the Boltzmann constant) and I_ν is the Fermi integral [33] of order ν. The screened potential $\Phi[n_e(\mathbf{r})]$ is related to the electronic density $n_e(\mathbf{r})$ by [32]

$$n_e(\mathbf{r}) = \frac{\sqrt{2}}{\pi^2\beta^{\frac{3}{2}}}\, I_{\frac{1}{2}}\big(\Phi[n_e(\mathbf{r})]\big); \tag{5}$$

charge conservation constrains the integral $\int d\mathbf{r}\, n_e(\mathbf{r})$ to be equal to the total electronic charge.

The first integral in Eq. (4), which depends only on the local electronic density n_e in the true spirit of the Hohenberg-Kohn theorem [34], is the well-known finite-temperature Thomas-Fermi expression [35]. The exchange-correlation term $F_{xc}[n_e]$ is expressed in the local density approximation of Perdew and Zunger [36, 37]. For this study, we omit the von Weiszäcker correction and work in a Thomas-Fermi-Dirac form using the formula proposed by Perrot [38] to represent the kinetic-entropic part. The divergence of the electron-nucleus potential is regularized at each thermodynamic condition through a procedure that closely follows the production of the norm-conserving pseudopotential for QMD [16]. The cutoff radius is chosen to be 30% of the Wigner-Seitz radius, sufficient to prevent overlap of the regularization spheres. The number of plane waves describing the local electronic density is then adjusted to converge the thermodynamic properties to within less than 1%.

At each time step, the electronic free energy is minimized in terms of the local electronic density. The ions are propagated as in the QMD method with the same number of atoms, N_i = 54. Upon input of the mass density, the volume of the cubic simulation cell is determined from the atomic weight (A=244) for Pu. The time steps, determined from the thermal velocity of the nuclei and the Wigner-Seitz radius [39], varied from 2.5 fs at the highest

temperature (5 keV) to 5.0 fs at the lowest temperature (50 eV) with a maximum of 20,000 steps.

C. Transport properties

The self-diffusion coefficient D can be computed from the trajectory (so-called equilibrium molecular dynamics, EMD) by the mean-square displacement

$$D = \frac{1}{6t}\left\langle \left|\mathbf{R}_i(t) - \mathbf{R}_i(0)\right|^2 \right\rangle \tag{6}$$

or by the velocity autocorrelation function

$$D = \frac{1}{3}\int_0^\infty \left\langle \mathbf{V}_i(t)\cdot\mathbf{V}_i(0)\right\rangle \, \mathrm{d}t \ , \tag{7}$$

where $\mathbf{R}_i$ ($\mathbf{V}_i$) is the position (velocity) of the i$^{\text{th}}$ nucleus. These two formulations of the self-diffusion coefficients are formally equivalent in the long-time limit. We have generated trajectories of sufficient temporal length to reach times such that the velocity autocorrelation function becomes zero and contributes no further to the integral, and the mean-square displacement away from the origin consistently fits to a straight line. Since the values obtained from these two approaches generally lie within one percent of each other, we report only one value.

The shear viscosity

$$\eta = \lim_{t\to\infty} \overline{\eta}(t), \tag{8}$$

is computed from the autocorrelation function (Green-Kubo relation) of the off-diagonal component of the stress tensor [40],

$$\overline{\eta}(t) = \frac{V}{k_B T}\int_0^t \left\langle P_{12}(0)P_{12}(t')\right\rangle \, \mathrm{d}t'. \tag{9}$$

The precision is somewhat improved by averaging the results for the five independent off-diagonal components of the stress tensor, P_{xy}, P_{yz}, P_{zx}, $(P_{xx}-P_{yy})/2$, and $(P_{yy}-P_{zz})/2$.

Unlike the self-diffusion coefficient, which involves only single-particle correlations and attains significant statistical improvement from averaging over the particles, the viscosity depends on the entire system and therefore requires very long trajectories in order to achieve the desired statistical accuracy. We have previously found [17] that empirical fits to the integrals of the autocorrelation functions can substantially shorten the length of the trajectory

required. In turn, extrapolation of the fits to $t \to \infty$ can more effectively determine the basic dynamical properties. The partial integrals of the off-diagonal stress-tensor autocorrelation function $\overline{\eta}(t)$, Eq. (9), have been fit to an arbitrary functional form $A[1 - e^{-(\frac{t}{\tau})^n}]$, where A and τ are free parameters with A giving the desired property in the $t \to \infty$ limit and the power n is either 1 (exponential) or 2 (gaussian). Fitting to this form at short-time integrations produces reasonable approximations to η. This fitting procedure also serves to damp long-time fluctuations.

The fractional statistical error in computing a correlation function C from molecular-dynamics trajectories [41] is given by

$$\frac{\Delta C}{C} = \sqrt{\frac{2\tau}{T_{\text{traj}}}}, \tag{10}$$

where T_{traj} is the length of the trajectory and τ is the correlation, or e-folding, time of the function, calculated from the fit or from interrogations of the function itself. In the present work, we generally fit over the interval $[0,\tau]$ or $[0,2\tau]$ for $n = 1$ or $n = 2$, respectively. This interval emphasizes the fit in the region where the function varies most quickly; as t increases, the statistics become poorer since there are fewer time origins to sum over when constructing the autocorrelation function [40]. The computed statistical error in the viscosity is 10% or less, but a total uncertainty of $\sim 20\%$ is estimated by experience due to the fitting procedure and extrapolation to infinite time. The statistical error in the self-diffusion coefficient is smaller than for viscosity since the particle average gives an additional $1/\sqrt{N_i}$ factor.

To aid in the analysis of the simulation results, we will consider three simple models/phenomenological forms for describing transport: kinetic theory, the Arrenhius equation, and the Stokes-Einstein relation. For the kinetic theory of hard spheres, a model that is most appropriate for dilute atomic and molecular gasses, $D_{\text{HS}} \propto n_i^{-1} T^{1/2}$ and $\eta_{\text{HS}} \propto T^{1/2}$.

The Arrenhius equation describes the general behavior of a quantity as function of the temperature over a certain range as

$$A(T) = A_0 e^{-E_A/k_B T}, \tag{11}$$

where E_A represents an activation energy for the initiation of the process, A_0 is a pre-factor setting the magnitude, and k_B is the Boltzmann constant. This expression has found broad

application to a variety of processes from diffusion to the viscosity of liquid metals [42] such as U, Au, and Pb, as well as chemical rates.

The Stokes-Einstein relation gives a connection between the diffusion and shear viscosity though an expression

$$F_{SE}[D,\eta] \equiv \frac{D\eta}{k_B T {n_i}^{1/3}} = C_{SE}, \tag{12}$$

with C_{SE}, a constant and F_{SE}, a shorthand notation for the relationship between the transport coefficients. Various prescriptions [43] exist for determining the constant C_{SE}. From the original derivations based on the motion of a test particle through a solvent, C_{SE} ranges from $1/6\pi$ (0.053) [44] to $1/4\pi$ (0.080) [45] depending on the limits of the slip coefficient from infinity (stick) to zero (slip) respectively. On the other hand, Chisolm and Wallace [46] determined an empirical value of 0.18 ± 0.02, in a global fit to 21 metal species from a theory of liquids near melt. We shall examine to what extent these phenomenological forms represent the behavior of Pu over the various regimes we explore.

D. INFERNO/OCP model

The classical one component plasma (OCP) presents a idealized model in which point ions interact through the Coulomb potential within a neutralizing background of electrons. Large-scale molecular dynamics and Monte Carlo simulations of the OCP [47–52] have demonstrated that many of the basic properties such as diffusion and viscosity can be represented in terms of a single quantity, the plasma coupling coefficient Γ, defined by the ratio of the potential to kinetic energy,

$$\Gamma = \frac{Z^2 e^2}{a k_B T}, \tag{13}$$

where Ze is the ion charge,

$$a = \left(\frac{3}{4\pi n_i}\right)^{1/3} \tag{14}$$

is the ion-sphere radius, and $n_i = \rho/M$ is the number density for ions of mass M and mass density ρ . Systems in which the ratio exceeds unity ($\Gamma > 1$) are designated as strongly coupled with the particle interactions dominating the thermal motion. The fits of the dynamical properties in terms of Γ range in complexity from a simple power law to elaborate functions of power series. For example, Hansen *et. al.* [52] give

$$\frac{D}{\omega_p a^2} = 2.95\Gamma^{-1.34} \tag{15}$$

with

$$\omega_p = (4\pi n_i/M)^{\frac{1}{2}} Ze \tag{16}$$

the ion plasma frequency. Even this simple form masks a complex dependence on the density and temperature as evinced through the ionic parameters a, Γ, and ω_p. For the Pu temperature and density ranges investigated in this paper, we employ the more complicated fits of Daligault [51] for D and of Bastea [47] for η. A more comprehensive study of the various OCP calculations and fits appears in our earlier paper on DT mixtures [14].

The OCP model applies strictly to a fully-ionized system; however, for the temperatures and densities in this study, plutonium ($Z = 94$) remains only partially ionized. Therefore, modifying the charge in such a manner as to reflect the ionization degree may permit an extension of the OCP formulas to cooler realms. A reasonable choice involves replacing Z in Eq. (13) with an effective charge $\bar{Z}$ determined from a more realistic representation of an atom within the plasma [53]. For this task, we employed the computer code INFERNO [18], which solves the Dirac equation in a self-consistent-field approximation assuming a finite temperature and an average atom. Continuum states are treated on the same basis as bound states, and "continuum lowering" is automatically included. The high-density limit is essentially the Thomas-Fermi-Dirac model, and the low-density limit yields ions in equilibrium with free electrons. The effective charge given by INFERNO is shown in Fig. 1 as a function of temperature for the three representative densities. As expected, $\bar{Z}$ increases with increasing temperature; however, the curves for different densities cross as a function of temperature exhibiting the importance of both pressure and temperature on ionization. We emphasize that, for the remainder of the paper, we shall employ the label "INFERNO/OCP" to designate that the OCP viscosities and diffusion coefficients have been calculated with Z replaced by $\bar{Z}$ to allow for partial ionization effects.

As Γ gives an indication of the relative importance of particle interactions and motion, the electron Fermi degeneracy parameter Θ gauges the importance of quantum effects. This parameter is defined as the ratio of the temperature to the nonrelativistic Fermi energy as

$$\Theta = k_B T / E_F \tag{17}$$

where

$$E_F = \hbar^2 \frac{(3\pi^2 n_e)^{2/3}}{2m_e} \tag{18}$$

with n_e and m_e the electron number density and electron mass respectively. For $\Theta < 1$, the system becomes degenerate, and quantum mechanics begins to play an increasingly important role in the modeling of the system. We caution though that Γ basically characterizes a classical system and Θ derives from a non-interacting model of the electrons, and therefore both should be viewed as semi-quantitative guides.

III. RESULTS AND DISCUSSION

A. Liquid plutonium

In Fig. 2, we compare the experimentally-measured [4, 6] viscosity of liquid plutonium with results from our QMD simulations (N_i=54) and the previous MEAM calculations [8]. A liquid density of ρ_L =17.4 g/cm^3 was used in the QMD simulations at all four temperatures. This scaled QMD density accounts in some measure for the difference between DFT and acutal Pu measurements. Using the ratio of the thermodynamic to QMD atomic volumes for δ-Pu yields a scaled QMD density of 16.2 g/cm^3, close to the range of reported experimental values for liquid Pu at melt [16.3-16.7 g/cm^3] and at 1223 K [16.19 g/cm^3]. By comparison, the MEAM simulations predict a density of 17.29 g/cm^3 at a melting temperature of 918 ± 5 K. The empirical MEAM potential enables simulations of a larger number of atoms in a cell than QMD, and MEAM calculations were performed with both equilibrium molecular dynamics (EMD) and nonequilibrium, shear-driven molecular dynamics (NEMD). The two approaches agreed in the limits in which the NEMD was extrapolated to zero shear rate and the EMD was extended to long times. We note that, for a Leonard-Jones fluid, no size dependence for the calculated shear viscosity was found [54] for $N_i \geq 27$. A spot check for OFMD simulations of uranium at ambient density for temperatures ranging between 200 and 1000 eV showed a sensitivity of 11% or less between samples of $N_i = 54$ and 75 (such a difference can be attributed to the fitting procedure discussed above). Referring to Fig. 2, the QMD results are about 40% lower than the experiment while the MEAM results are 3-4 times higher than the experiment, making the MEAM viscosities 4 to 7 times larger than the QMD. In both cases, the differences with the experimental values are considerably larger than the theoretical error bars (no error bars were given in the report of the experiment). As can be seen from the points falling approximately on a straight line

in the semilogrithmic plot, the results of both calculations, as well as the experiment, are fit fairly well by an Arrhenius form. For the Arrhenius parameters, the agreement between experiment vs. QMD is quite good: E_A = -0.13 vs. -0.11 eV and A_0 = 1.09 vs. 0.98 mPa-sec. In comparison, for the MEAM simulations: E_A = -0.2 eV and A_0 = 1.8 mPa-sec.

No experimental results exist for the diffusion constants of plutonium. The results of the present QMD calculation and the MEAM (done with EMD only) calculation are shown in Fig. 3. The QMD diffusion constants are about three to seven times larger than the MEAM values. Again, both are well fit by an Arrhenius form. The Arrhenius parameters for the QMD and MEAM are respectively E_A = 0.13 and 0.37 eV; $A_0 = 9.4 \times 10^{-5}$ and 2.5×10^{-4} cm^2/sec. Thus the QMD results decay more slowly with temperature as compared to the MEAM results.

B. Plutonium in the intermediate regime

In the previous section, we examined the behavior of plutonium at liquid densities and temperatures up to 1500K. We now raise the temperature while remaining near liquid density ($\sim$ 20 g/cm^3) in order to enter the warm dense matter regime. For plutonium in the range of 1 to 5 eV, Γ ranges from about 550 to 150 and Θ varies from about 0.015 to 0.06, with both calculated using $Z = \bar{Z}$. Thus the medium becomes both strongly coupled and degenerate with quantum mechanical effects expected to play a major role. The QMD and OFMD results for D and η are shown in Figs. 4 and 5 as a function of temperature for two densities: (1) ρ_L = 17.4 g/cm^3, the "DFT-scaled" liquid density, for QMD (see earlier discussion) and (2) 1.5 ρ_L = 26.2 g/cm^3 for both QMD and OFMD.

We first examine the QMD results at liquid density, ρ_L. The diffusion coefficient shows a monotonic rise with increasing temperature although with some changes of slope. However, the viscosity displays a clear change in character as a function of temperature. Just above the melting temperature, the viscosity decreases with increasing T with an Arrhenius behavior ($\sim e^{-E_\eta/k_BT}$ with $E_\eta < 0$) typical of a liquid metal, whereas at higher temperatures, the viscosity steadily rises with temperature, resembling the behavior of a hard-sphere fluid or a partially-ionized one-component plasma. This behavior occurs in other systems, even for the simplest case of hydrogen [55], and represents a shift from processes dominated by the potential interactions to those controlled by the kinetics. The diffusion coefficient has only

a kinetic component related to the correlations in position or velocity while the stress tensor contains contributions both from the motion and potential interactions of the particles. Therefore, the change in the nature of the fluid as the temperature rises becomes more apparent in the viscosity. This competition leads to a distinct minimum in the viscosity at around $T \sim 0.4$ eV.

In addition, this transition regime provides an excellent testbed for comparing the QMD and OFMD approaches. Due to the number of active electrons and the increasing number of states required for the diagonalization of the KS equations, the QMD becomes computationally prohibitive above about 5 eV with our choice of parameters. On the other hand, the need to represent detailed quantum mechanical interactions begins to wane as the temperature rises so that the OFMD at the TFD level gains greater validity. To this end, we have compared the QMD and OFMD at the higher density (1.5 ρ_L), as displayed in Figs. 4 and 5. The results for the two formulations between 2 and 4 eV agree closely to within the statistical error bars for both D and η. While comparison over a wider regime in temperature and density as with DT [14] and iron [16] would provide additional confirmation, the close correspondence in magnitude and behavior tends to corroborate the OFMD approximation and its extension to higher densities and temperatures.

In Fig. 6, we plot the Stokes-Einstein expression $F_{SE}[D, \eta]$ as a function of temperature, using the diffusion coefficients and viscosities from the OFMD at $1.5\rho_L$ and the QMD at ρ_L and $1.5\rho_L$. Within the expected fitting error of $\sim 20\%$ for determining viscosity from the simulations, the QMD and the OFMD results show relatively good agreement and are bounded by the classical values of C_{SE} from below and the Chisolm-Wallace liquid metal value from above. The function $F_{SE}[D, \eta]$ for the QMD at the lower density (ρ_L) evinces a sharp decline at the lowest temperatures. The near linear rise of the diffusion coefficient with temperature in this region basically cancels the temperature dependence of the denominator, leaving the behavior of F_{SE} dominated by the viscosity and thus reflecting its sharp decline at low temperature as shown in Fig. 5. As discussed above, this sharp bend in the viscosity with temperature reflects a change from potential to kinetic dominated regimes. This steep decline is exaggerated by the point at 900 K. If we disregard the value at 900 K near the experimental melting point, then the QMD results between $T = 1100$ and 40000 K for both densities are close to a constant value of $C_{SE}= 0.11 \pm 0.01$. Omitting the lowest temperature seems reasonable since the melting temperature for Pu as predicted by QMD is not known,

as too many atoms would be required to perform a moving interface [56] melting simulation with a reasonable amount of computational resources. The OFMD results for the higher density also remain almost constant with $C_{SE} \sim 0.1$.

C. Plutonium in the dense-plasma regime (above 50 eV)

The self-diffusion coefficient D and the shear viscosity η are shown in Figs. 7 and 8, respectively, for plutonium at temperatures between 50 eV and 5 keV and densities between 20 and 100 g/cm^3 or approximately solid density to five times compressed. Both transport properties increase with temperature in this range. The diffusion coefficient decreases with increasing density while the viscosity increases with increasing density.

The Stokes-Einstein relation of D and η, given by Eq. (12), is shown in Fig. 9. The quantity F_{SE} is only weakly dependent on temperature and density, with an average value around 0.075. This value is larger than the stick value of $1/6\pi$ (=0.053) but close to that for slip $1/4\pi$ (=0.080) for a Brownian fluid. It is smaller than found for plutonium in the liquid or WDM regimes (see previous sections). We note that F_{SE} is much more nearly constant as a function of density and temperature than found in our recent study [14] on the DT mixture in the WDM regime.

The INFERNO/OCP model results are shown as dashed curves in Figs. 7, 8, and 9 for comparison with the OFMD calculations. With $\bar{Z}$ calculated with INFERNO, Γ ranges from 26 to 71 for the temperatures and densities considered. At solid density the INFERNO/OCP results are within about 40% of the OFMD results at the calculated temperatures, the OFMD being the smaller for both diffusion and viscosity. In the higher density cases (3 and 5 times solid density), the agreement is similar to that at high temperatures; however, the INFERNO/OCP results deviate from the OFMD results with a different slope at the lower temperatures. The INFERNO/OCP values of F_{SE}, shown in Fig. 9 by the open data points, are larger than given by the OFMD calculations but show the same tendencies with temperature and density.

Some simplified models or limiting cases, such as the hard-sphere approximation, predict power-law dependences on temperature and density. Though such formulas are certainly oversimplified, we have attempted to fit our numerical data on viscosity η and self diffusion D in the whole temperature and density range using similar forms but different exponents.

The resulting least-squares fits are

$$D_{\rm fit} = a_D T^{b_D} (\rho/\rho_0)^{c_D} \ \ {\rm cm}^2/{\rm sec} \tag{19}$$

with $a_D = 0.000239 \pm 0.000022$, $b_D = 0.548 \pm 0.014$, and $c_D = -0.383 \pm 0.023$, and

$$\eta_{\rm fit} = a_\eta T^{b_\eta} (\rho/\rho_0)^{c_\eta} \ \ {\rm mPa\ sec} \tag{20}$$

with $a_\eta = 3.13 \pm 0.26$, $b_\eta = 0.360 \pm 0.010$, and $c_\eta = 0.780 \pm 0.034$, where T is in eV and ρ is in g/cm^3. The fit of the viscosity is shown in Fig. 10. These simple formulas fit all the calculated points to within $\sim 30\%$, except for those at T=50 eV and $\rho/\rho_0 = 1$. The fits improve as T increases. For $T \geq 300$ eV, the deviations of the fits from the data are less than 10%. The temperature and density scaling of F_{SE} [Eq. (12)] predicted by the least-square fits is nearly constant, weakly scaling as $\mathrm{T}^{-0.092}$ and $\rho^{0.064}$, respectively. Though the deviations of the fits from the actual data are sometimes greater than the statistical errors, the fits should be satisfactory for many purposes.

IV. SUMMARY

We have calculated the self-diffusion coefficients and viscosities of plutonium from liquid to dense plasmas states by employing two quantum mechanical molecular dynamics approaches: (1) a finite-temperature density functional theory in the Kohn-Sham formulation and generalized gradient approximation (QMD); and (2) an orbital-free method at the Thomas-Fermi-Dirac level (OFMD). For reference, we also employed a one component plasma (OCP) model with an effective charge determined from the average-atom program INFERNO.

For the liquid state, we found the QMD viscosity was lower by about 40% than experiment [4] and lower by by a factor of 4 to 7 than molecular dynamics simulations using a modified embedded atom method (MEAM) [8]. Both the viscosity and diffusion coefficients exhibit Arrhenius behaviors with the QMD activation energy for the viscosity agreeing well with experiment but about 40% lower than the MEAM calculation. At intermediate temperatures (1–5 eV), the QMD and OFMD results for diffusion and viscosity agree to within $\sim 20\%$. The viscosity has a minimum at $T \approx 0.4$ eV, corresponding to the transition from a liquid into the warm, dense matter regime. For dense plasmas conditions (T = 50 eV to 5 keV,

$\rho = 1 - 5$ times solid density), both the diffusion coefficient and viscosity increase with increasing temperature. With increasing density, the diffusion coefficient decreases while the shear viscosity η increases.

A Stokes-Einstein relation between the viscosity and diffusion coefficient holds reasonably well for both the WDM and dense plasma regimes although with different constants: $C_{SE} \approx 0.13$ and 0.075, respectively. In the dense plasma regime, the transport properties of the modified OCP agree with the OFMD to within $\sim 40\%$ at solid density (~ 20 g/cm^3) but show greater departures at higher densities and lower temperatures. A simple analytic fit of the calculated diffusion coefficient and viscosity is provided.

Acknowledgments

We wish to acknowledge useful conversations and suggestions by Brad Holian, Frank Cherne, John Wills, Sven Rudin, Eric Schwegler, and Carl Greeff. We specially thank Flavien Lambert for providing his OFMD code and for continued consultations on the use of the OFMD code. This work was supported by the Advanced Simulation and Computing Program and Campaign 4. The Los Alamos National Laboratory is operated by Los Alamos National Security, LLC for the National Nuclear Security Administration of the U.S. Department of Energy under Contract No. DE-AC52-06NA25396.

---

[1] S. S. Hecker and M. Stan, J. Nucl. Mat. **383**, 112 (2008).

[2] V. P. Bobkov *et al.*, *Thermophysical Properties of Materials for Nuclear Engineering: A Tutorial and Collection of Data* (IAEA, Vienna, 2008), Sect. 2.2, pp. 14–21.

[3] S. P. Rudin, Phys. Rev. B **76**, 195424 (2007) and references therein.

[4] L. J. Wittenberg, D. Ofte, and W. G. Rohr, Nucl. Appl. Technol. **3**, 550 (1967).

[5] R.I. Sheldon, G. H. Rinehart, J. C. Lashley, C. E. Van Pelt, P. C. Nordine, S. Krishnon, and J. K. R. Weber, J. Nucl. Mat. **312**, 207 (2003).

[6] L. V. Jones, D. Ofte, W. G. Rohr, and L. J. Wittenberg, Trans. Am. Soc. Metals **55**, 819 (1962).

[7] L. J. Wittenberg, D. Ofte, W. G. Rohr, and D. V. Rigney, Metallurgical and Materials Trans-

actions B **2**, 287 (1971).

[8] F. J. Cherne, M. I. Baskes, and B. L. Holian, Phys. Rev. B **67**, 092104 (2003).

[9] F. J. Cherne, M. I. Baskes, and P. A. Deymier, Phys. Rev. B **65**, 024209 (2001).

[10] D. Alfe, and M. J. Gillan, Phys. Rev. Lett. **81**, 5161 (1998).

[11] G. A. de Wijs, G. Kresse, L. Vocadlo, D. Dobson, D. Alfe, M. J. Gillan, Nature (London) **392**, 805 (1998).

[12] J. D. Chai, V. L. Ligneres, G. Ho, E. A. Carter, and J. D. Weeks, Chem. Phys. Lett. **473**, 263 (2009).

[13] G. Zérah, J. Clérouin and E. L. Pollock, Phys. Rev. Lett. **69**, 446 (1992).

[14] J. D. Kress, J. S. Cohen, D. A. Horner, F. Lambert, and L. A. Collins, Phys. Rev. E **82**, 036404 (2010).

[15] F. Lambert, J. Clérouin and S. Mazevet, EPL **75**, 681 (2006).

[16] F. Lambert, J. Clérouin and G. Zérah, Phys. Rev. E **73**, 016403 (2006).

[17] D. A. Horner, F. Lambert, J.D. Kress, and L.A. Collins, Phys. Rev. B **80**, 024305 (2009).

[18] D. A. Liberman, J. Quant. Spectrosc. Radiat. Transfer **27**, 335 (1982).

[19] G. Kresse and J. Hafner, Phys. Rev. B **47**, 558 (1993).

[20] G. Kresse and J. Furthmuller, Comput. Mat. Sci. **6**, 15 (1996).

[21] G. Kresse and J. Furthmuller, Phys. Rev. B **54**, 11169 (1996).

[22] P. H. Hünenberger, Adv. Polym. Sci. **173**, 105 (2005).

[23] R. M. Martin, *Electronic Structure: Basic Theory and Practical Methods* (Cambridge University Press, Cambridge, England, 2004).

[24] J. P. Perdew, J. A. Chevary, S. H. Vosko, K. A. Jackson, M. R. Pederson, D. J. Singh, and C. Fiolhais, Phys. Rev. B **46**, 6671 (1992).

[25] D. C. Wallace, Phys. Rev. B **58**, 15433 (1998).

[26] O. Eriksson, J. D. Becker, A. V. Balatsky, and J. M. Wills, J. Alloys Compd. **287**, 1 (1999).

[27] S. Y. Savrasov, G. Kotliar, and E. Abrahams, Nature (London) **410**, 793 (2001).

[28] P. Soderlind and B. Sadigh, Phys. Rev. Lett. **92**, 185702 (2004).

[29] J. C. Lashley, A. Lawson, R. J. McQueeney, and G. H. Lander, Phys. Rev. B **72**, 054416 (2005).

[30] J. Clérouin, E. L. Pollock, G. Zérah, Phys. Rev. A **46**, 5130 (1992).

[31] S. Mazevet, F. Lambert, F. Bottin, G. Zérah, and J. Clérouin, Phys. Rev. E **75**, 056404 (2007).

[32] F. Lambert, J. Clérouin, J.-F. Danel, L. Kazandjian, and G. Zérah, Phys. Rev. E **77**, 026402 (2008).

[33] S. Ichimaru, *Statistical Plasma Physics, Vol. II: Condensed Plasmas* (Addison-Wesley, Reading, MA, 1994), Appendix B.

[34] P. Hohenberg and W. Kohn, Phys. Rev. **136**, B864 (1964).

[35] M. Brack and R. K. Bhaduri, *Semiclassical Physics* (Westview Press, Boulder, CO, 2003).

[36] J. P. Perdew and A. Zunger, Phys. Rev. B **23**, 5048 (1981).

[37] G. Faussurier, P. L. Silvestrelli, and C. Blancard, High Energy Density Phys. **5**, 74 (2009).

[38] F. Perrot, Phys. Rev. A **20**, 586 (1979).

[39] P. Vieillefosse and J. P. Hansen, Phys. Rev. A **12**, 1106 (1975).

[40] M. P. Allen and D. J. Tildesley, *Computer Simulation of Liquids* (Oxford University Press, New York, 1987).

[41] R. Zwanzig and N. K. Ailawadi, Phys. Rev. **182**, 280 (1969).

[42] D. Ofte, J. Nuclear Mats. **22**, 28 (1967).

[43] M. Cappelezzo, C. A. Capellari, S.H. Pezzin, and A.F. Coehlo, J. Chem. Phys. **126**, 224516 (2007).

[44] A. Einstein, Z. Elektrochem. **14**, 235 (1908).

[45] W. Sutherland, Phil. Mag. **9**, 781 (1905).

[46] E. Chisolm and D. Wallace, *Shock Compression of Condensed Matter – 2005*, edited by M. D. Furnish, M. Elert, T. P. Russell, and C. T. White, CP845 (American Institute of Physics, New York, 2006).

[47] S. Bastea, Phys. Rev. E **71**, 056405 (2005).

[48] F. Lambert, Ph.D. thesis, Université Paris XI–Commissariat à l'Énergie Atomique, 2007.

[49] B. Bernu and P. Vieillefosse, Phys. Rev. A **18**, 2345 (1978).

[50] Z. Donkó, B. Nyíri, L. Szalai, and S. Holló, Phys. Rev. Lett. **81**, 1622 (1998); Z. Donkó and B. Nyíri, Phys. Plasmas **7**, 45 (2000).

[51] J. Daligault, Phys. Rev. Lett. **96**, 065003 (2006); **103**, 029901(E) (2009).

[52] J. P. Hansen, I. R. McDonald, and E. L. Pollock, Phys. Rev. A **11**, 1025 (1975).

[53] D. Giles, F. Lambert, J. Clerouin, and G. Salin, High Eng. Den. Phys. **3**, 95 (2007) and references therein.

[54] I.-C. Yeh and G. Hummer, J. Phys. Chem B **108**, 15873 (2004).

[55] J. Clerouin, J. Phys.: Condens. Matter **14**, 9089 (2002).

[56] M. I. Baskes, Phys. Rev. B **62**, 15532 (2000).

TABLE I: QMD results for liquid plutonium ($\rho = 17.4$ g/cm^3, scaled to correspond to experiment) self-diffusion coefficients and viscosities. The error bars are statistical only. Numbers in brackets represent powers of ten.

T (K)	η (mPa s)	D (cm^2/s)
900	3.83 ± 0.15	1.8[-5]
1100	2.91 ± 0.12	2.1[-5]
1300	2.74 ± 0.11	2.8[-5]
1500	2.11 ± 0.08	3.6[-5]
2901	1.24 ± 0.05	1.2[-4]
6847	1.37 ± 0.07	2.3[-4]
10212	1.75 ± 0.09	2.8[-4]
12766	1.94 ± 0.08	3.3[-4]

TABLE II: QMD results for plutonium self-diffusion coefficients and viscosities at $\rho = 26.1$ g/cm^3. The error bars are statistical only. Numbers in brackets represent powers of ten.

T (eV)	η (mPa s)	D (cm^2/s)
0.50	3.6 ± 0.2	9.5[-5]
1.00	4.3 ± 0.3	1.6[-4]
1.50	4.8 ± 0.3	2.0[-4]
2.00	5.5 ± 0.2	2.6[-4]
2.34	5.5 ± 0.3	3.1[-4]
3.00	5.8 ± 0.2	3.5[-4]
3.50	6.2 ± 0.3	4.0[-4]
4.00	6.7 ± 0.3	4.3[-4]
4.50	6.5 ± 0.5	4.9[-4]

TABLE III: OFMD results for plutonium self-diffusion coefficients and viscosities at $\rho = 26.1$ g/cm^3. The error bars are statistical only. Numbers in brackets represent powers of ten.

T (eV)	η (mPa s)	D (cm^2/s)
2.00	7.3 ± 0.3	2.0[-4]
3.00	6.3 ± 0.3	3.0[-4]
4.00	6.0 ± 0.2	3.9[-4]
5.00	6.3 ± 0.3	4.3[-4]

TABLE IV: Self-diffusion coefficients D and viscosities η, determined by OFMD, and the values of $\bar{Z}$, determined by Inferno, used in the OFMD calculations. $\rho_1 = 20$ g/cm^3.

ρ/ρ_1	T (eV)	η (mPa s)	D (cm^2/s)	$\bar{Z}$
1	50	8.3	0.00293	12.24
1	100	12.1	0.00389	17.59
1	200	15.5	0.00518	24.51
1	300	23.3	0.00594	30.66
1	500	29.1	0.00735	40.01
1	600	30.6	0.00786	43.76
1	650	33.5	0.00818	45.19
1	700	36.6	0.00851	47.04
1	750	34.9	0.00864	48.54
1	800	35.8	0.00886	50.14
1	1000	42.0	0.00993	55.03
3	50	22.8	0.00140	17.04
3	100	32.1	0.00215	21.16
3	200	45.7	0.00303	25.39
3	300	54.1	0.00371	28.84
3	500	68.8	0.00436	38.02
3	750	87.3	0.00558	46.00
3	1000	95.3	0.00640	51.49
3	5000	163.9	0.01710	83.60
4	5000	190.5	0.01490	83.07
5	200	71.9	0.00236	28.24
5	300	81.6	0.00291	30.75
5	500	101.6	0.00372	37.48
5	750	124.7	0.00448	45.35
5	1000	149.3	0.00513	50.87
5	5000	234.3	0.01350	82.30

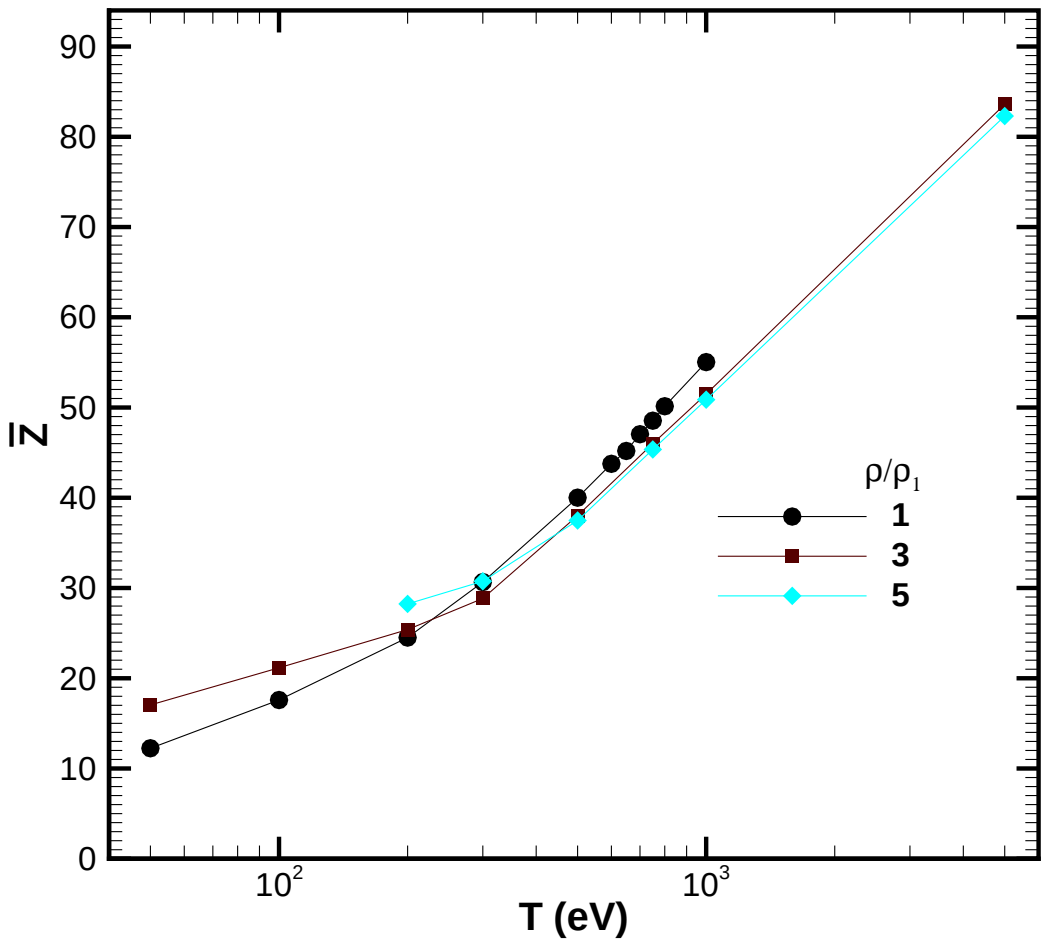

FIG. 1: (Color online) Effective charge $\bar{Z}$ for plutonium determined by the code INFERNO [18]. $\bar{Z}$ is shown as a function of temperature for densities 20 (ρ_1), 60, and 100 g/cm^3, denoted by circles, squares, and diamonds, respectively.

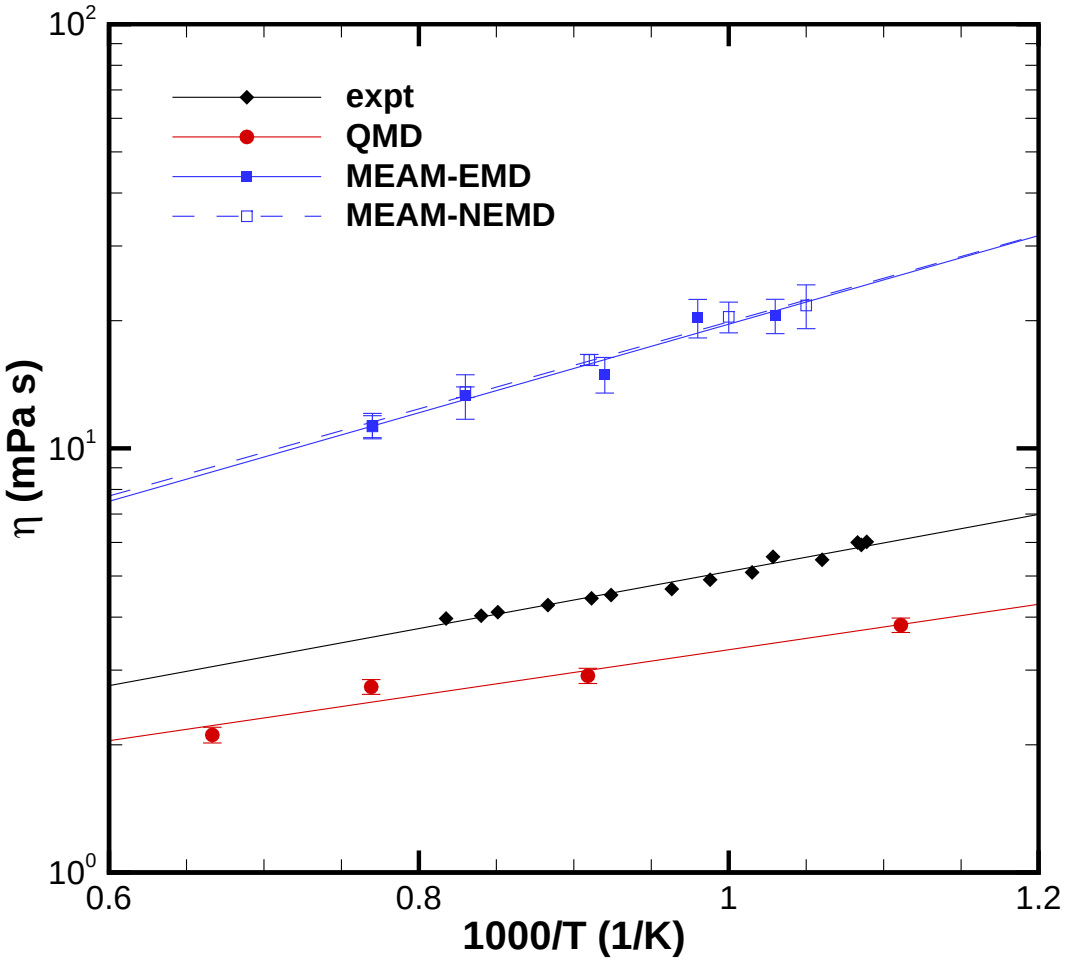

FIG. 2: (Color online) Shear viscosity of liquid plutonium as a function of inverse temperature: experimental results (diamonds, no error bars were given) [4]; present QMD calculations (circles, with statistical error bars); MEAM calculations [8] by equilibrium molecular dynamics (EMD, solid squares) and by nonequilibrium molecular dynamics (NEMD, open squares). The straight lines are exponential (Arrhenius) fits to the data points.

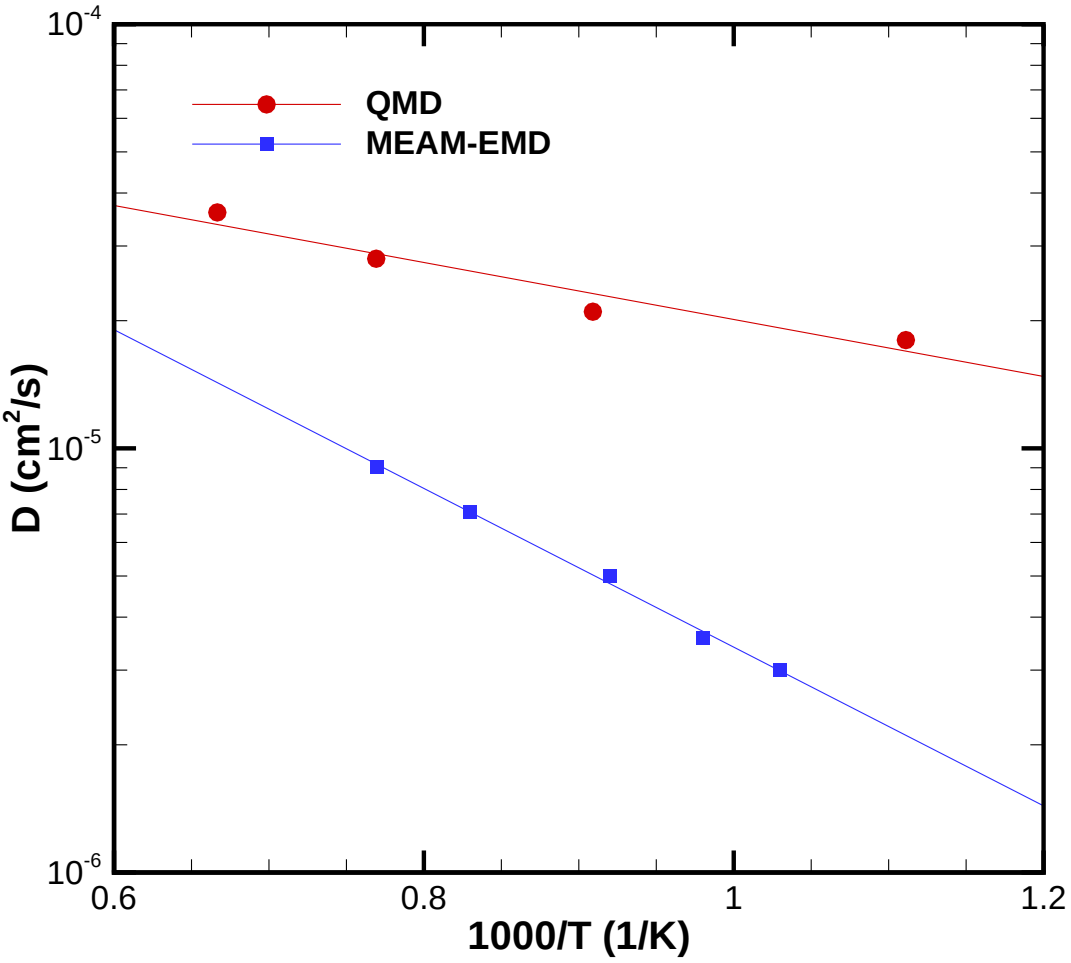

FIG. 3: (Color online) Diffusion coefficient of liquid plutonium as a function of inverse temperature: present QMD calculations (circles) and MEAM calculations with equilibrium molecular dynamics (squares) [8]. The straight lines are exponential (Arrhenius) fits to the data points.

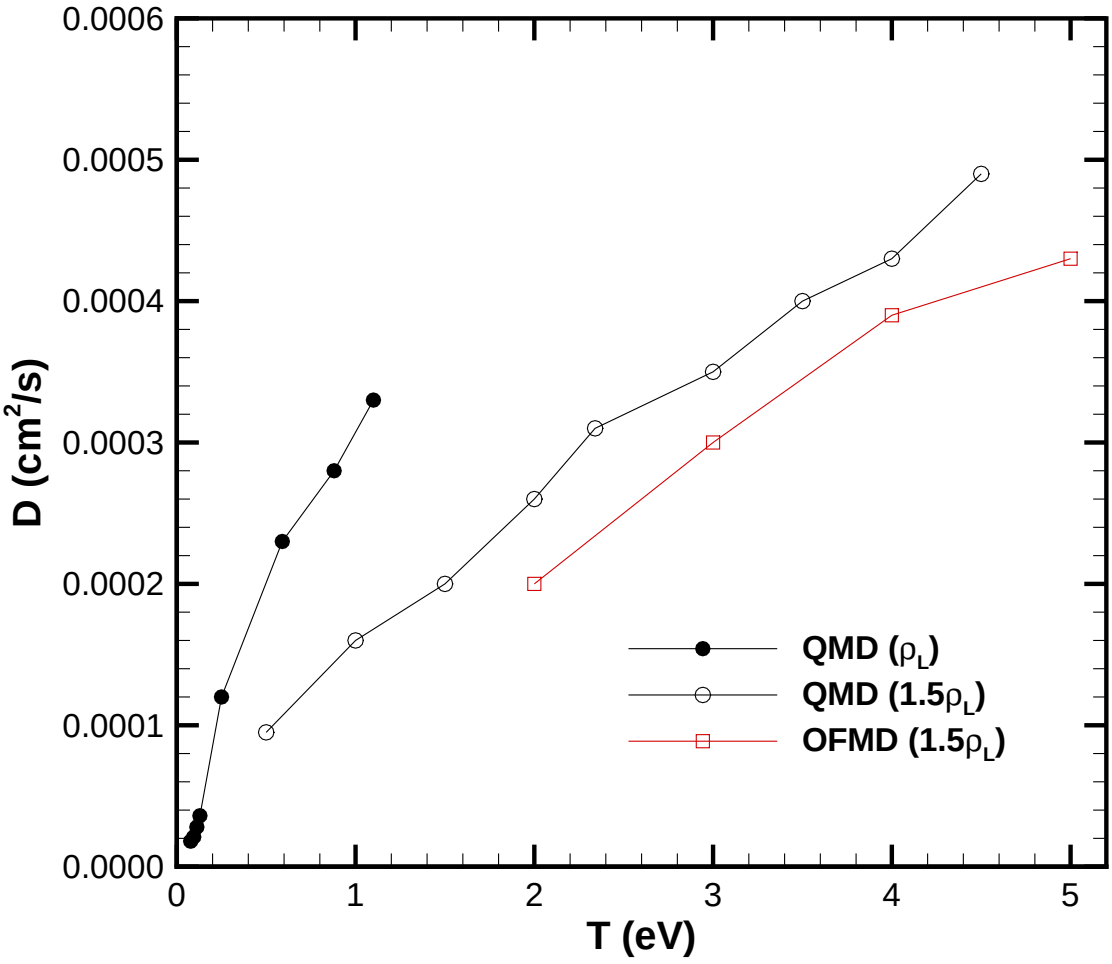

FIG. 4: (Color online) Diffusion coefficients of plutonium as a function of temperature in the WDM regime, calculated by the QMD method for densities of 17.4 g/cm^3 (ρ_L; solid circles) and 26.1 g/cm^3 (1.5 ρ_L; open circles) and by the OFMD method at density 26.1 g/cm^3 (1.5ρ_L; open squares). The straight line segments between data points are provided to guide the eye only.

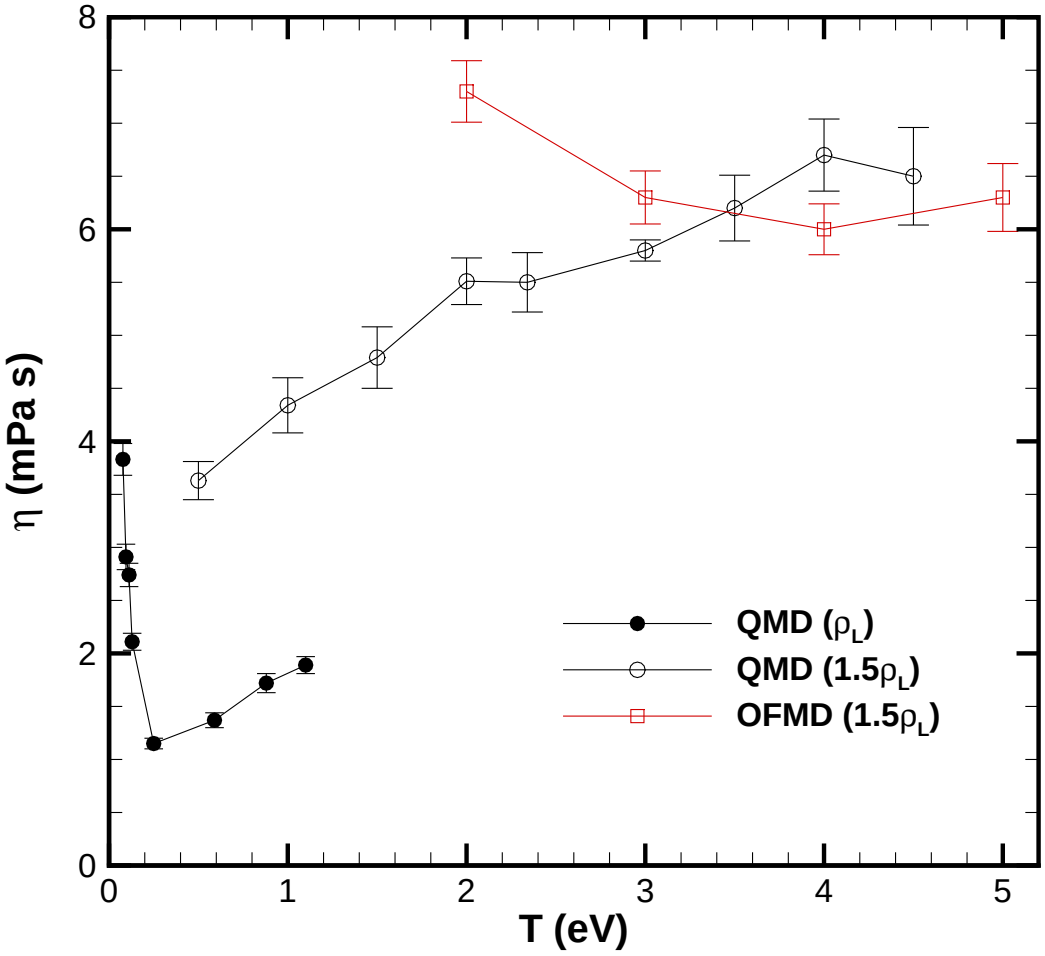

FIG. 5: (Color online) Viscosities of plutonium as a function of temperature in the WDM regime, calculated by the QMD method for densities of 17.4 g/cm^3 (ρ_L; solid circles) and 26.1 g/cm^3 (1.5 ρ_L; open circles) and by the OFMD method at density 26.1 g/cm^3 (1.5 ρ_L; open squares). The straight line segments between data points are provided to guide the eye only and the error bars are statistical only.

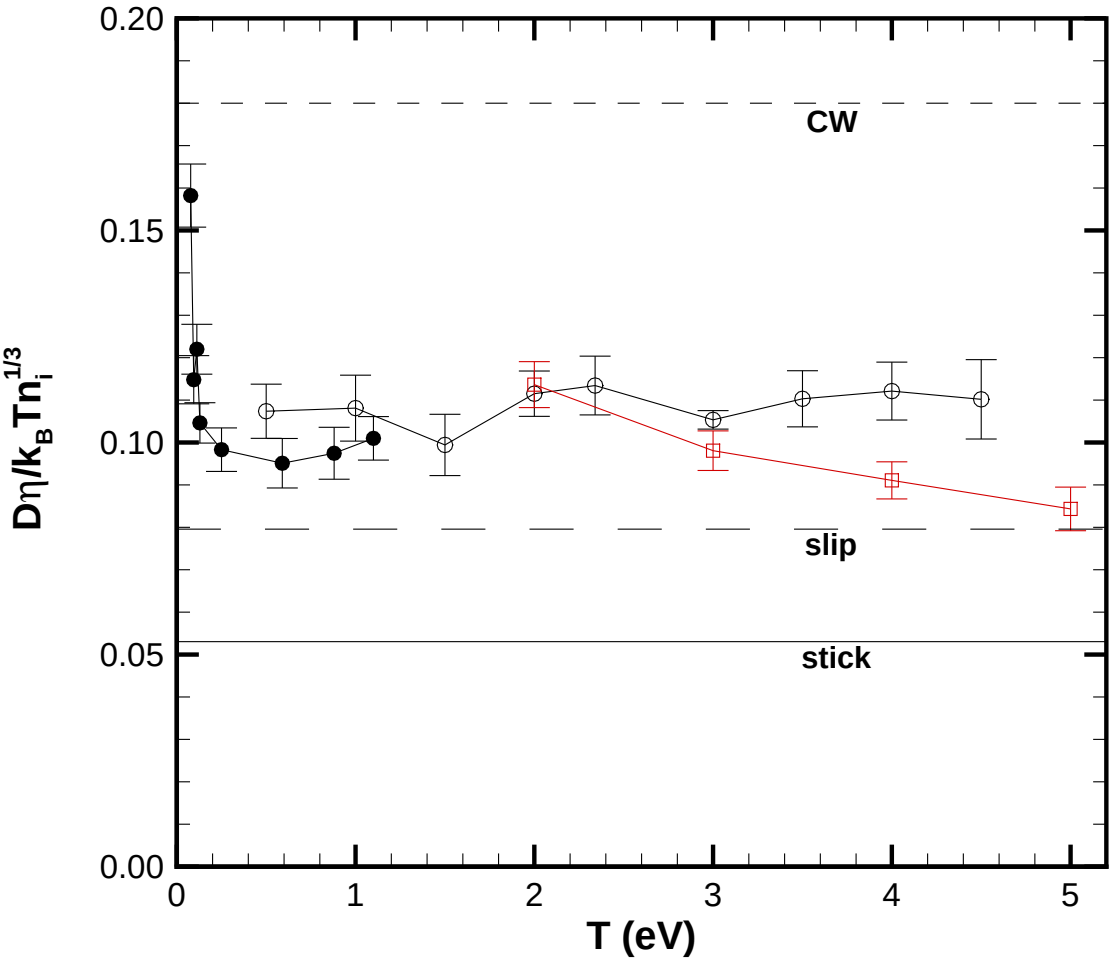

FIG. 6: (Color online) Stokes-Einstein relation F_{SE} as a function of temperature for the diffusion coefficients and viscosities shown in Figs. 4 and 5. The error bars are statistical only, and the straight line segments between data points are provided to guide the eye only. The flat lines show the constant values of C_{SE} for stick (solid) and slip (long dashed) boundary conditions as well as the empirical result of Chisolm and Wallace [46] (short dashed). The designations of the curves are the same as in Figs. 4 and 5.

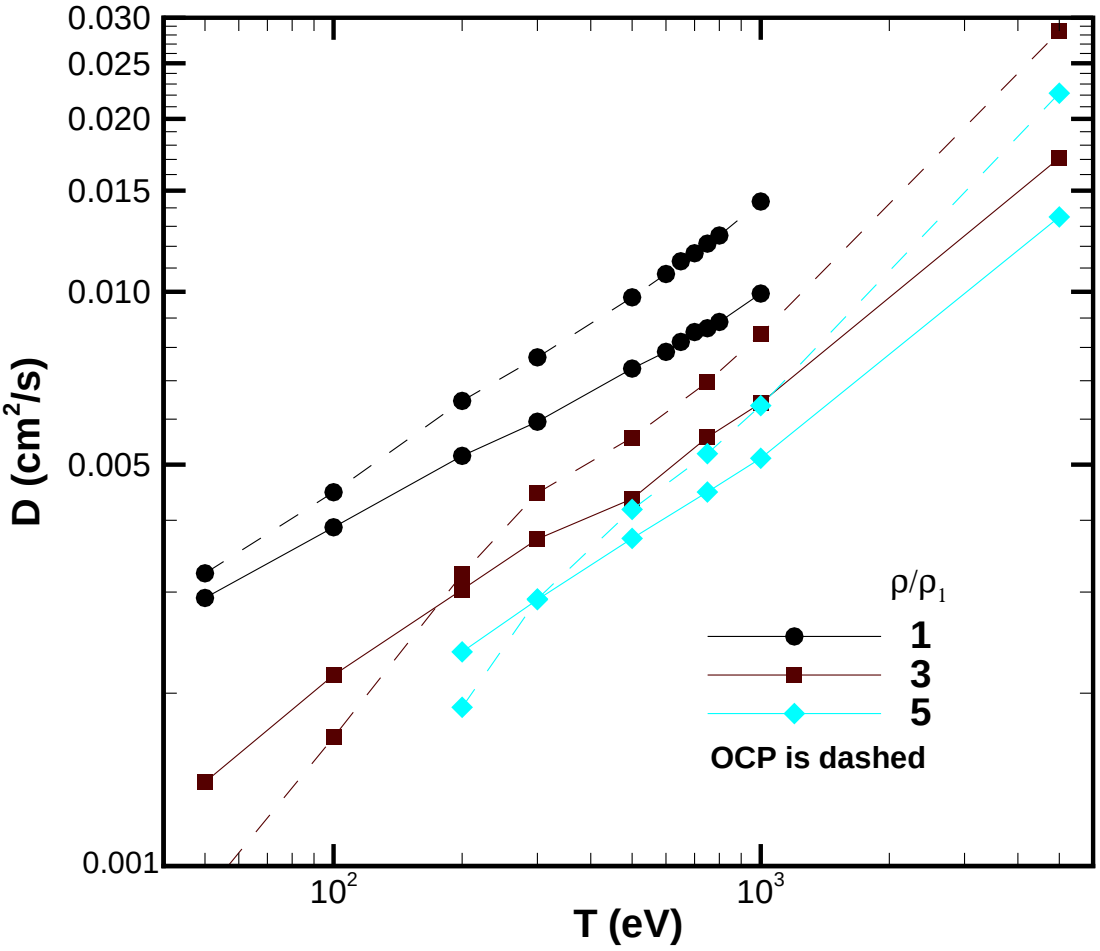

FIG. 7: (Color online) Self-diffusion coefficients of dense-plasma plutonium, calculated by OFMD, as a function of temperature for densities 20 (ρ_1), 60, and 100 g/cm^3. The dashed lines connect points calculated by the INFERNO/OCP model.

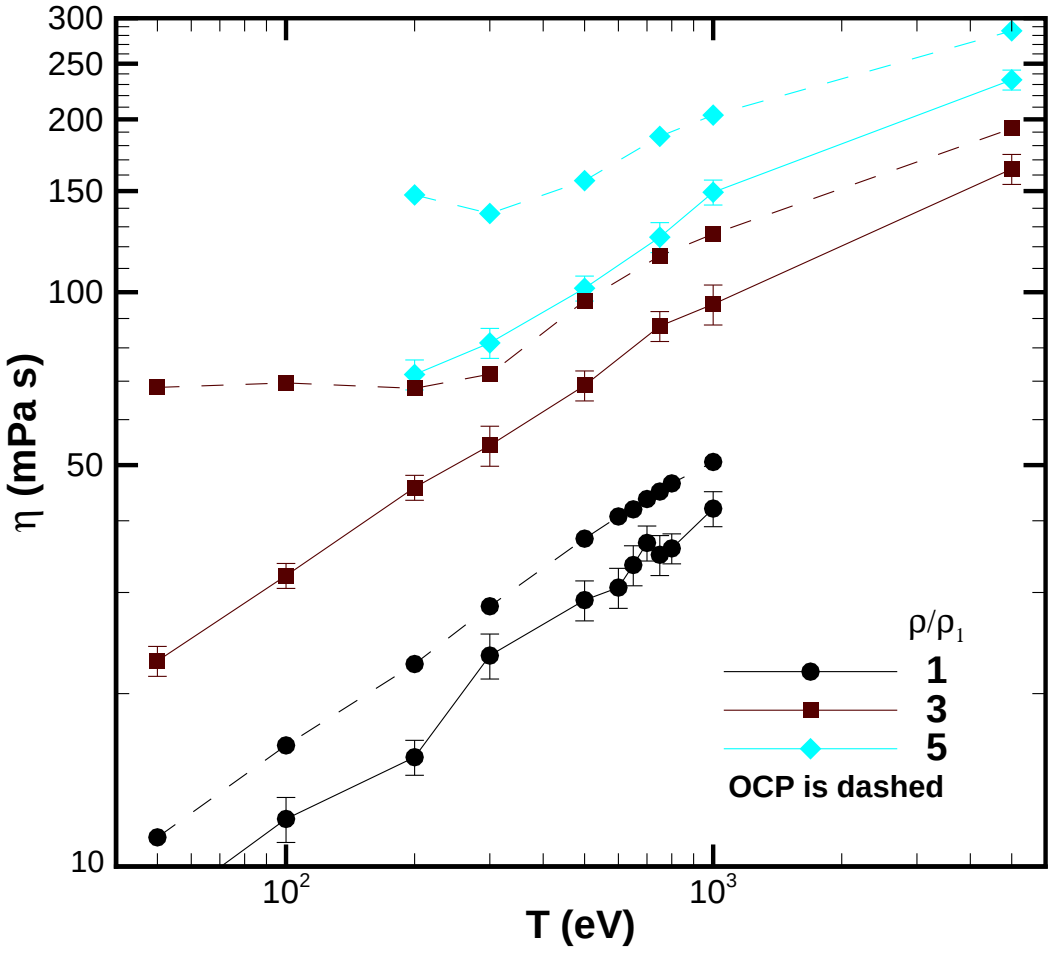

FIG. 8: (Color online) Shear viscosities of dense-plasma plutonium, calculated by OFMD, as a function of temperature for densities 20 (ρ_1), 60, and 100 g/cm^3. The dashed lines connect points calculated by the INFERNO/OCP model.

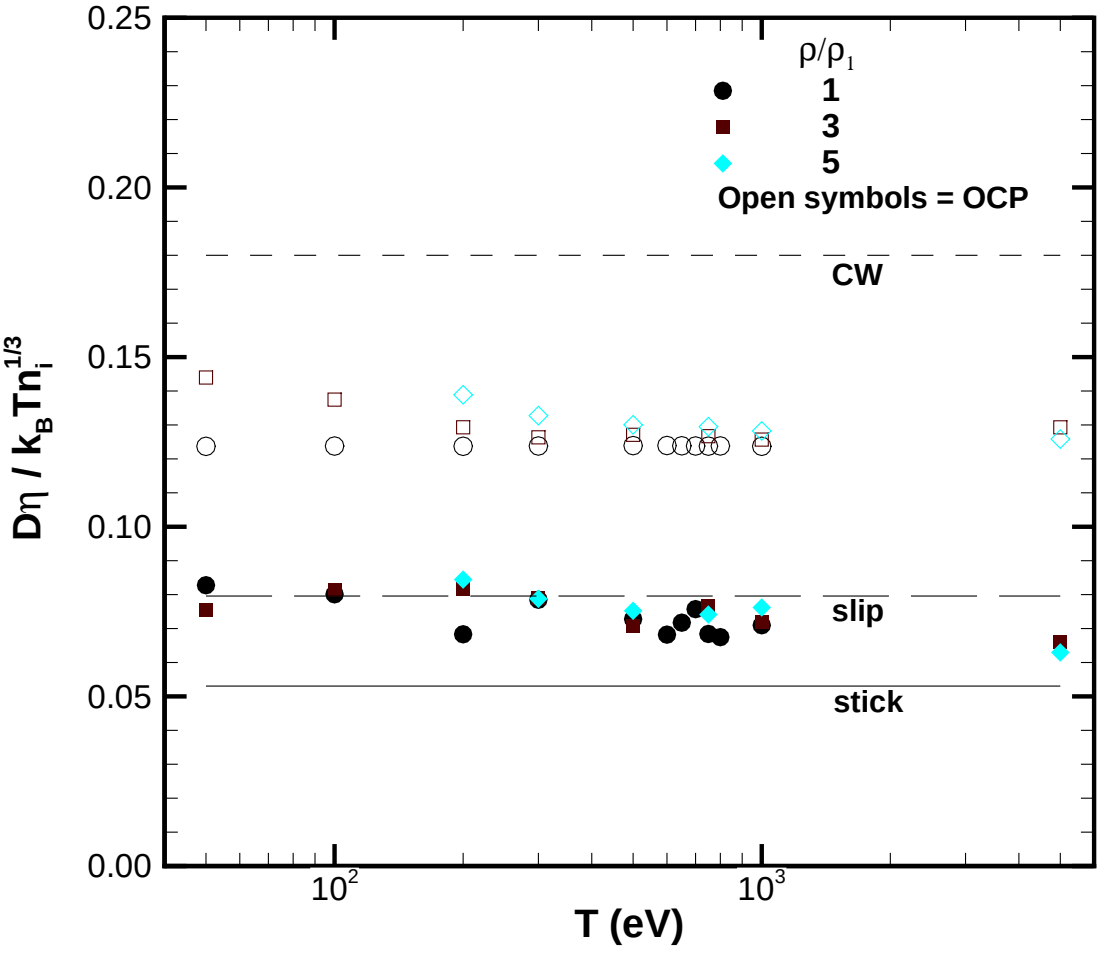

FIG. 9: (Color online) Stokes-Einstein relation F_{SE} as a function of temperature for the diffusion coefficients and viscosities shown in Figs. 7 and 8. The closed symbols are the results of the OFMD calculations and the open symbols are the results of the INFERNO/OCP model. The flat lines show the constant values of Stokes-Einstein for stick (solid) and slip (long dashed) boundary conditions as well as the empirical result of Chisolm and Wallace [46] (short dashed).

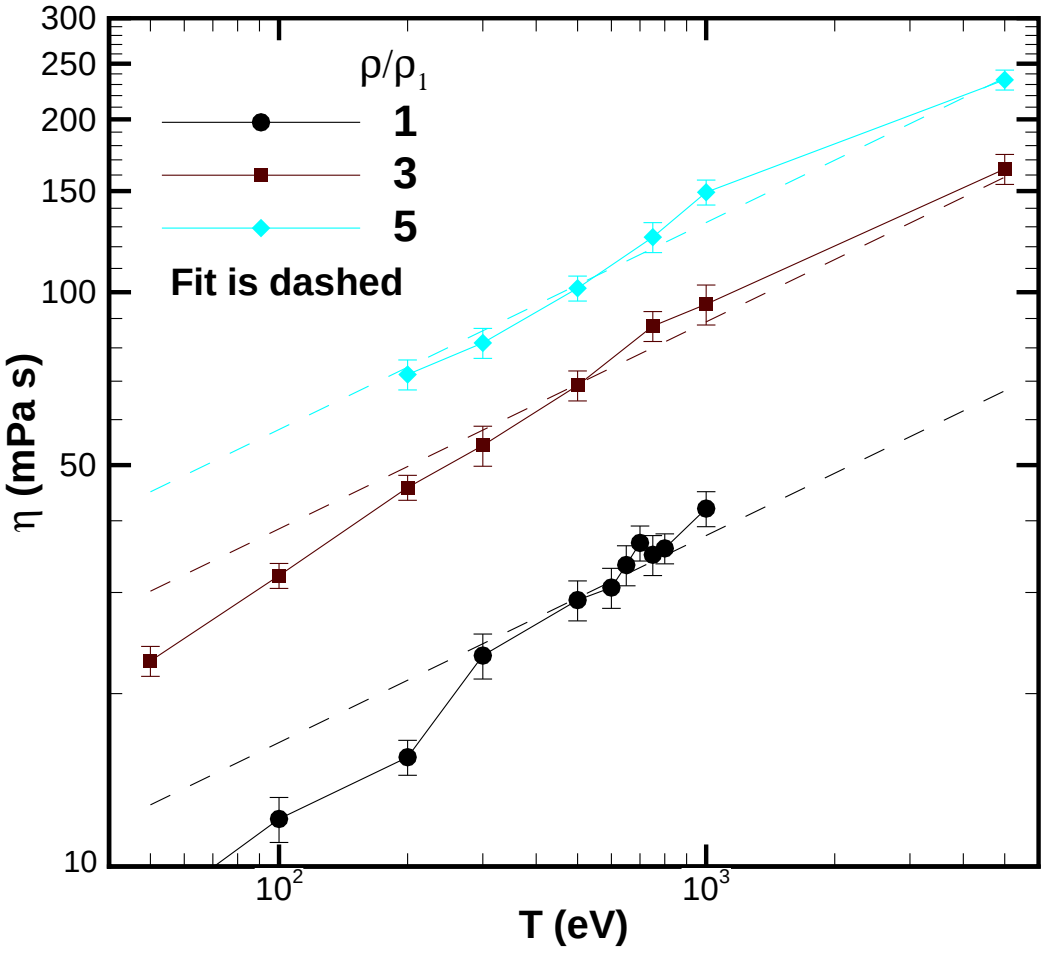

FIG. 10: (Color online) Shear viscosities of dense-plasma plutonium with fits (dashed) by Eq. 20.